Cell Metabolism
Article

Loss of White Adipose Hyperplastic Potential Is Associated with Enhanced Susceptibility to Insulin Resistance

Soo M. Kim,[1] Mingyue Lun,[1] Mei Wang,[2] Samuel E. Senyo,[3,4,5] Christelle Guillermier,[1,2,4] Parth Patwari,[3,4] and Matthew L. Steinhauser[1,3,4,5,*]
[1]Department of Medicine, Division of Genetics, Brigham and Women's Hospital, Boston, MA 02115, USA
[2]National Resource for Imaging Mass Spectroscopy, Brigham and Women's Hospital, Cambridge, MA 02138, USA
[3]Department of Medicine, Division of Cardiovascular Medicine, Brigham and Women's Hospital, Boston, MA 02115, USA
[4]Harvard Medical School, Boston, MA 02115, USA
[5]Harvard Stem Cell Institute, Cambridge, MA 02138, USA
*Correspondence: msteinhauser@partners.org
http://dx.doi.org/10.1016/j.cmet.2014.10.010

SUMMARY

Fat mass expansion occurs by adipocyte hypertrophy or recruitment of differentiating adipocyte progenitors, the relative balance of which may impact systemic metabolism. We measured adipogenesis in murine subcutaneous (sWAT) and visceral white adipose tissue (vWAT) using stable isotope methodology and then modeled adipocyte turnover. Birth and death rates were similar within depots; however, turnover was higher in vWAT relative to sWAT. In juvenile mice, obesity increased adipogenesis, but in adults, this was only seen in vWAT after prolonged high-fat feeding. Statistical modeling suggests differentiation of adipocyte progenitors without an accompanying self-renewing division step may partially explain the age-dependent decline in hyperplastic potential. Additional metabolic interrogation of obese mice demonstrated an association between adipocyte turnover and insulin sensitivity. These data therefore identify adipocyte hypertrophy as the dominant mechanism of adult fat mass expansion and support the paradoxical concept that metabolic disease ensues due to a failure of adipose tissue plasticity.

INTRODUCTION

The accepted paradigm of fat cell development holds that self-renewing adipocyte progenitors differentiate into mature lipid-storing adipocytes (Berry and Rodeheffer, 2013; Gupta et al., 2012; Rodeheffer et al., 2008; Tang et al., 2008). Although fat mass expansion may occur by generation of new fat cells (hyperplasia) or hypertrophy of existing adipocytes, the role of adipocyte hyperplasia at different developmental stages and with obesity is incompletely elucidated. Indeed, estimates of adult homeostatic adipogenesis vary by nearly two orders of magnitude (Jo et al., 2009; Neese et al., 2002; Rigamonti et al., 2011; Spalding et al., 2008; Wang et al., 2013). Moreover, while some studies suggest a role for adipocyte hyperplasia in the fat pad expansion seen with obesity (Ellis et al., 1990; Johnson et al., 1978; Lemonnier, 1972; Neese et al., 2002; Rigamonti et al., 2011), cytometric analyses (Hood and Allen, 1977; Salans et al., 1971, 1973) and recent ^{14}carbon birth-dating experiments (Spalding et al., 2008) suggest that adipocyte number is fixed in adulthood.

Here, we adapted stable isotope methodology to measure adipogenesis, using thymidine, enriched to a high concentration (~97%) with the rare stable isotope of nitrogen (^{15}N) as a tracer for cell division (Steinhauser et al., 2012). While conceptually similar to using radiolabeled thymidine or halogenated nucleotide analogs, stable isotopes provide several advantages (Steinhauser and Lechene, 2013; Stürup et al., 2008). First, stable isotopes are innocuous and therefore not associated with potential artifact from reagent toxicity. Second, observations made in model organisms can be tested with translational human studies due to the extensive precedent of safe human application. Third, mass spectrometry allows measurement of stable isotope tracers with high precision. In this study, we utilized isotope ratio mass spectrometry (IRMS) to measure tracer uptake in cell fractions isolated from adipose tissue and multi-isotope imaging mass spectrometry (MIMS) to quantitatively image stable isotopes in histologic sections. MIMS merges the precise tracer measurements with imaging resolution approaching transmission electron microscopy (Lechene et al., 2006; Steinhauser et al., 2012). We measured adipogenesis during aging and in obesity models, guided by the rationale that quantifying the dynamics of adipogenesis—and therefore testing for an association between adipogenesis and fat mass expansion—is a vital step in determining the role of adipocyte turnover in the pathophysiology of obesity.

RESULTS

Stable Isotope Methodology to Track Adipogenesis In Vivo

We measured incorporation of ^{15}N-thymidine in replicating cells by an increase in ^{15}N/^{14}N above the natural ratio (0.37%), using two complementary mass spectrometry approaches (Figure 1A), MIMS and IRMS. Quantitative mass images rendered by MIMS

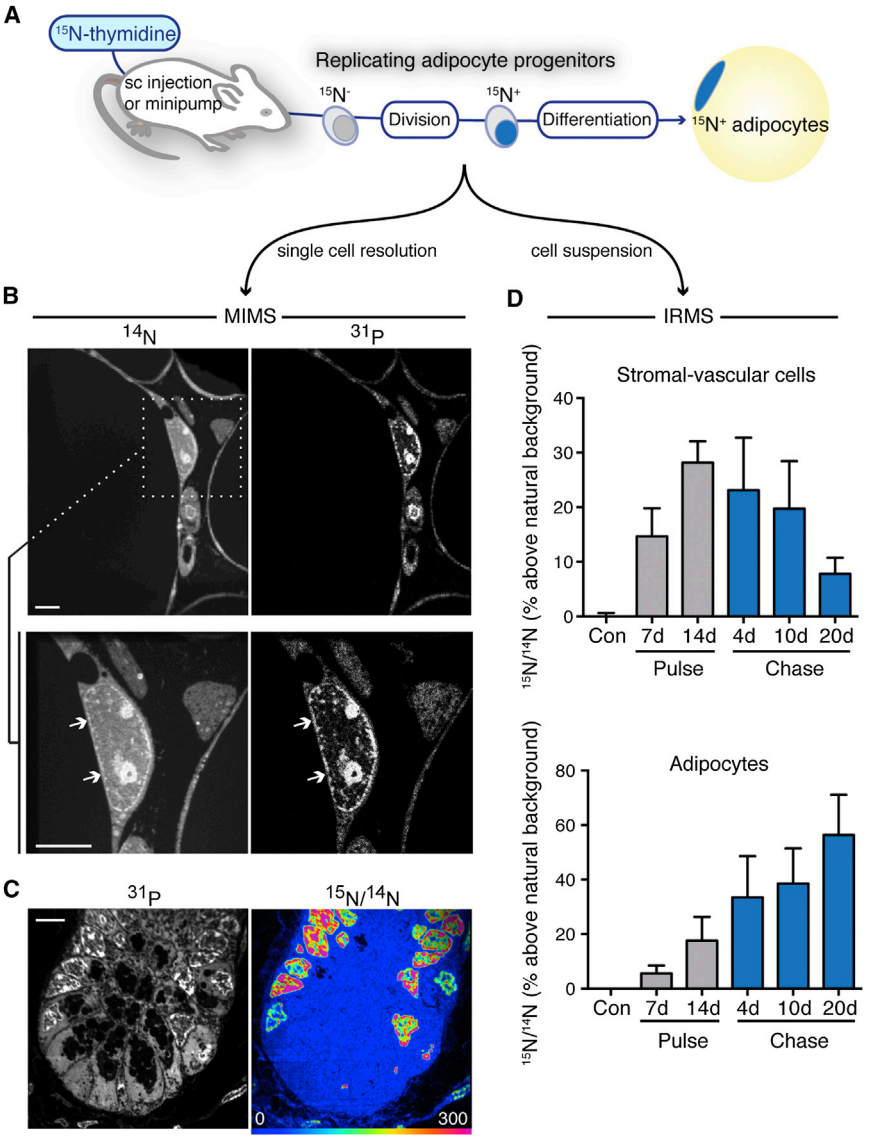

Figure 1. Tracking Adipogenesis in White Adipose Tissue with Stable Isotopes

(A) ^{15}N-thymidine labels dividing cells. (MIMS) measures label at the single cell level. Isotope ratio mass spectrometry (IRMS) is used for bulk analyses (e.g., a suspension of cells isolated from an individual depot).

(B) ^{14}N images show white tissue adipose (WAT) architecture and subcellular details, such as nuclei (white arrows). High phosphorus content in membranes and chromatin accounts for signal in ^{31}P images. Regions of interest (white box) can be reanalyzed at higher resolution. An adipocyte nucleus (white arrows) is seen adjacent to the lipid droplet, which has low nitrogen counts, and therefore appears dark. Scale bar represents 5 μm.

(C) Small intestinal crypt (+ control) after ^{15}N-thymidine. HSI ^{15}N/^{14}N image shows label localized to P-rich regions in the nucleus in a pattern resembling chromatin. The scale is set so blue is at natural abundance; blue regions (e.g., cytoplasm) are unlabeled. Scale bar represents 5 μm.

(D) Analysis of sWAT adipogenesis by ^{15}N-thymidine pulse-chase in 4-week-old mice (mean ± SEM; n = 3–4 mice per time point). Label taken up in the heterogeneous stromal vascular cell fraction (top) during pulse faded with chase, consistent with cell turnover. Adipocyte labeling trended upward ($p < 0.05$) during chase, consistent with differentiation of labeled progenitors into adipocytes. See also Figures S1 and S2.

reveal intracellular details, such as adipocyte nuclei, identifiable by their close association with a defining, large lipid droplet (Figure 1B and Figure S1 available online) and a shared plasma membrane. These features allow the discrimination of adipocytes from the less morphologically distinct and heterogenous interstitial cells, which include endothelial cells, fibroblasts, immune/inflammatory cells, and progenitors. For analyses described here, adipocyte identity was determined based on these morphologic criteria from mass images by an observer unaware of experimental group and labeling data.

Stable isotope measurements are visually rendered by a hue saturation intensity (HSI) transformation (Figure 1C) (Lechene et al., 2006). The low end (blue) of the scale is set to natural abundance and the upper bound (red) set to emphasize regional differences in tracer incorporation; however, scale changes leave the underlying quantitative data unmodified. The rapidly dividing small intestine serves as a positive labeling control (Figure 1C). ^{15}N-labeling is concentrated specifically in the nucleus (Senyo et al., 2013; Steinhauser et al., 2012). Labeling hotspots are observed throughout the nucleus, including condensed in close association to the nuclear membrane, a pattern expected of chromatin and comparable to that seen with DNA stains such as DAPI (Senyo et al., 2013). While we initially expected to see more cytoplasmic labeling due to mitochondrial DNA, this has not been evident even in mitochondrial rich tissues like the heart (Senyo et al., 2013), we speculate due to the extremely small size of the mitochondrial genome relative to nuclear DNA.

Although we previously detected rare cardiac myocyte division with MIMS, the analyses required ~1 year of instrument time (Senyo et al., 2013). WAT poses a similar challenge, due to the large size of adipocytes. A MIMS imaging plane (depth <1 nM) shows many adipocytes, however, adipocyte nuclei are infrequent. This provided rationale to use IRMS as a complementary, higher throughput approach. Analyses of WAT after pulse-chase administration of ^{15}N-thymidine to 4-week-old C57BL/6 mice, for example, showed increasing ^{15}N in adipocytes during chase, consistent with the differentiation of ^{15}N-labeled adipocyte progenitors; whereas, ^{15}N-signal in stromal-vascular cells from the same tissues showed a converse pattern of signal dilution, consistent with ongoing turnover (Figure 1D). In cell culture experiments, IRMS detected ^{15}N-thymidine labeling down to a frequency of ~1:500–1:1,000 cells

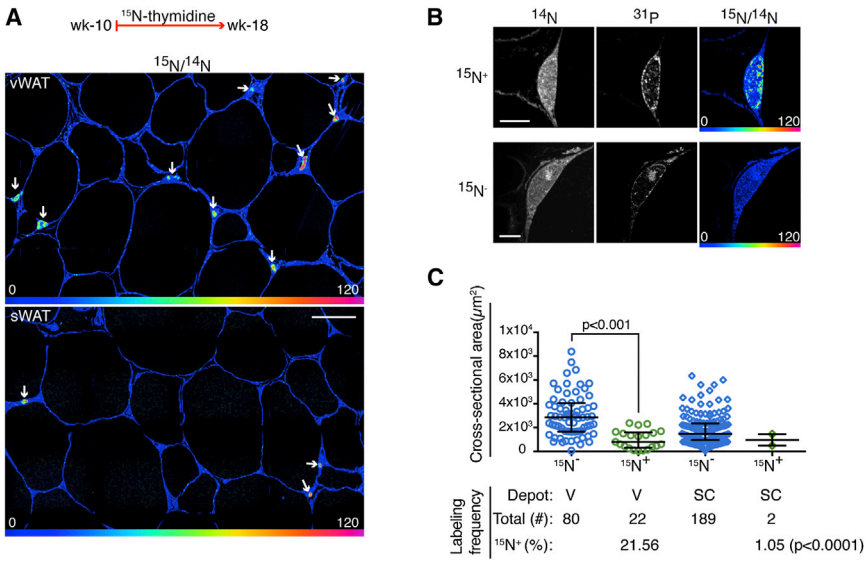

Figure 2. Depot-Specific Differences in Adult Adipogenesis

(A) ^{15}N-thymidine administered from postnatal weeks 10–18. Higher frequency of ^{15}N-nuclear labeling (white arrows) in vWAT (top) compared to sWAT (bottom). HSI mosaic images constructed from 60 μm tiles, scale bar represents 30 μm.

(B) Top: ^{15}N-labeled adipocyte. Bottom: ^{15}N-unlabeled adipocyte. Scale bar represents 5 μm.

(C) New (^{15}N^{+}) adipocytes are smaller than older (^{15}N^{-}) adipocytes as shown by area distribution. Bottom shows corresponding adipocyte labeling frequencies in the two depots. Pooled analysis of n = 3 mice.

See also Figures S3 and S4.

(Figure S2). Therefore, this approach combines the sensitivity to detect infrequent cell divisions with higher throughput, making it ideally suited to measure relative differences in adipogenesis.

Adult vWAT Demonstrates Increased Adipogenesis Relative to sWAT

To establish basal adipocyte formation in adult WAT, we labeled 10-week-old C57Bl/6 mice with ^{15}N-thymidine (20 μg/hr) for 8 weeks (Figure S3). Based on carbon birth-dating of human subcutaneous adipocytes, which showed an annual turnover rate of ~10% (Spalding et al., 2008), we predicted our analysis of 294 adipocyte nuclei would yield approximately five ^{15}N-labeled adipocytes. We detected 24 ^{15}N^{+} adipocyte nuclei (8.16%, pooled from n = 3 mice) (Figures 2A–2C); however, we also observed a marked interdepot difference. Whereas sWAT measurements were consistent with predictions from carbon birth dating (8 weeks: observed sWAT = 1.05%, expected = 1.54%, χ^2 p = 0.56), we found a higher rate of adipogenesis in vWAT (21.57% versus 1.05%, χ^2 p < 0.0001). ^{15}N^{+} adipocytes segregated into a distribution that was approximately normal (based on ^{15}N-intensity) and statistically distinct from the heterogenous stromal vascular cells (Figure S4). Stromal-vascular cells were also labeled at a significantly higher frequency (sWAT SV = 32%, n = 1,980; vWAT SV = 63%, n = 893) compared to adipocytes from the same depot (χ^2 p < 0.0001), consistent with a higher rate of stromal vascular cell turnover. ^{15}N^{+} adipocytes were also smaller than the unlabeled adipocytes (Figure 2C), consistent with the less mature state expected of recently differentiated adipocytes.

Cell division can also be measured during label-free chase by the predictable halving of label with each division (Steinhauser et al., 2012), an analysis made possible by quantitative sampling of nuclei (Figure S4). We therefore administered ^{15}N-thymidine to mice from postnatal day 4 through week 8 and analyzed WAT at two time points: at the end of the label and again after 18-month-long chase (Figure 3). Before chase, ^{15}N-labeling was detected in 56% and 85% of adipocytes in sWAT and vWAT, respectively (χ^2, p < 0.0001). Unlabeled adipocytes at this time point likely arose from cells that were committed to an adipocyte fate prior to the onset of labeling at postnatal day 4. Therefore, the higher frequency of unlabeled adipocytes in sWAT (44%) compared to vWAT (15%) is consistent with the previously shown earlier developmental age of sWAT compared to vWAT (Wang et al., 2013).

After the 18 month chase, in addition to an interval increase in adipocyte size (Figures 3A and 3B), vWAT labeling was dramatically reduced. While the dilution of label was particularly marked in the heterogeneous stromal-vascular fraction (Figure 3C), there was also significant dilution of label in visceral adipocytes (Figure 3C), consistent with the moderate turnover rate predicted by our measurements of adipogenesis rate in adult mice (Figure 2).

Unexpectedly, subcutaneous adipocytes displayed an opposite pattern. Rather than dilution of label, we observed a significant and paradoxical increase in the ^{15}N-labeled cells after the 18 month chase (Figure 3C, χ^2 p < 0.01). Because ^{15}N-labeled adipocytes were smaller than the ^{15}N^{-} adipocytes (Figure 2C), one hypothesis for the label enrichment is that the rate of cell death is higher in the larger, and likely older, ^{15}N^{-} cells. The surviving cells would then be more likely to be ^{15}N^{+}.

A second hypothesis for this pattern is that some adipocytes are formed from previously labeled adipocyte progenitors that then differentiated to generate new adipocytes without further division. In this case, the total adipocyte birth rate would be underestimated by pulse-labeling experiments. In addition, such a failure of progenitor self-renewal could lead to exhaustion of the pool, a phenomenon observed in genetic lineage tracing studies after prolonged administration of rosiglitazone, a PPARγ agonist, which is thought to promote adipogenesis (Tang et al., 2011).

Adipocyte Birth without Accompanying Progenitor Cell Division Is Required to Explain ^{15}N-label Dynamics in sWAT

To test which of the proposed hypotheses correctly explain the paradoxical enrichment of ^{15}N^{+} cells in the sWAT during the 18 month chase, we developed a model to simulate adipocyte ^{15}N label status, birth, and death over this period. The model combined the information obtained from the adult label experiment with the observations made at the beginning of the chase

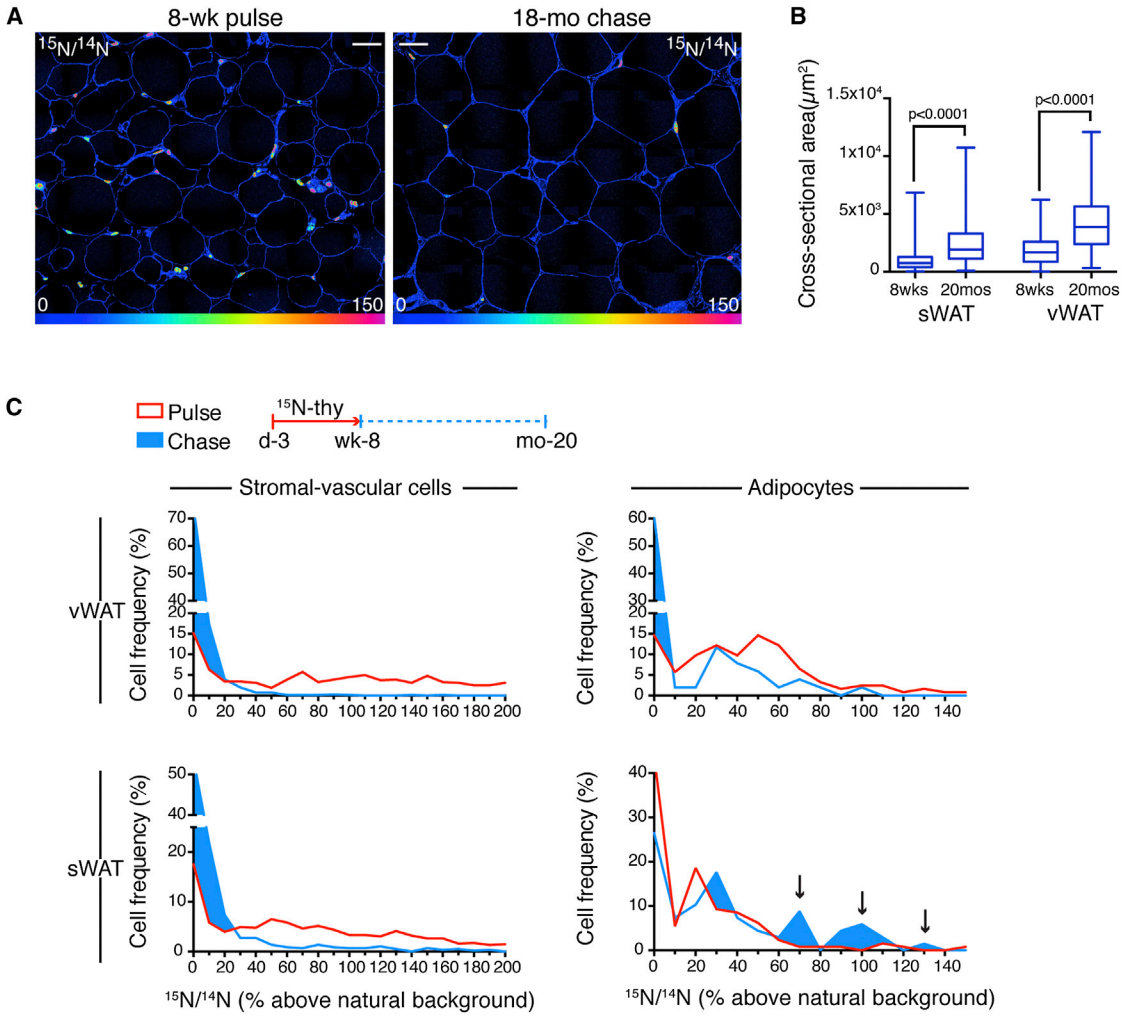

Figure 3. Limited Turnover of Subcutaneous Adipocytes with Aging

(A) ^{15}N-thymidine administered postnatal day 4 through week 8, followed by 18 month chase. WAT after pulse (left) and pulse-chase (right). ^{15}N-labeling is reduced with chase. Grossly larger adipocytes are seen in the old mice. HSI mosaic images constructed from 60 μm tiles. Scale bar represents 30 μm.

(B) Box plots of adipocyte size distributions as a function of age and depot (whiskers show max/min, n = 519–955 cells/depot).

(C) Frequency distributions after pulse (red) and pulse-chase (blue) as a function of nuclear labeling intensity (y axis). A significant downshift in stromal vascular cell labeling was seen in vWAT (V: top left) and sWAT (SC: bottom left) depots, consistent with turnover (χ^2 $p < 0.0001$). Visceral adipocytes (top right) also showed label dilution (χ^2 $p < 0.0001$), but to a lesser degree than SV cells (43% of adipocytes retaining label compared to 88% labeled after pulse). sWAT adipocytes (bottom right) paradoxically showed reverse dilution. The frequency of unlabeled adipocytes decreased (pulse = 44%; chase = 26%, χ^2 $p < 0.01$), due to an increase in highly labeled adipocytes (arrows). Pooled analysis of n = 3 mice/group.

See also Figures S3 and S5.

to simulate the effects of changing multiple assumptions. This allowed us to test multiple hypotheses for the observed enrichment of ^{15}N-positive cells in the sWAT, as well as test the sensitivity of our conclusions to the assumptions made.

For the baseline model, we initially assumed birth and death rates were equal, based on previous work (Jo et al., 2010). To validate this assumption, we experimentally determined adipocyte number and volume in mice of varying ages and found no significant variation in number over the time period of the chase (Figure S6). However, simulation demonstrated that varying the assumed relationship between birth and death from zero cell death to as much as 50% increased cell death, the baseline model could not explain more than a 3% enrichment in $^{15}N^+$ cells in the sWAT (Figures 4A and 4B; Table S1). We furthermore considered the possibility that due to cell heterogeneity, the observed proportion of $^{15}N^+$ cells in the SV compartment underestimates the true proportion of $^{15}N^+$ preadipocytes. However, simulations showed that even assuming that all preadipocytes were $^{15}N^+$ over the entire chase, the turnover rate in the sWAT was not high enough to cause more than a 7% enrichment in $^{15}N^+$ adipocytes ("Pread. all $^{15}N^+$," Figures 4A and 4B; Table S1).

Having rejected other hypotheses to explain the label enrichment, we incorporated into the model the increase in birth rate predicted in the case of adipocytes born without accompanying precursor cell division. Changing this assumption alone could explain an 8% enrichment in $^{15}N^+$ sWAT adipocytes ("f_{DS} = 1

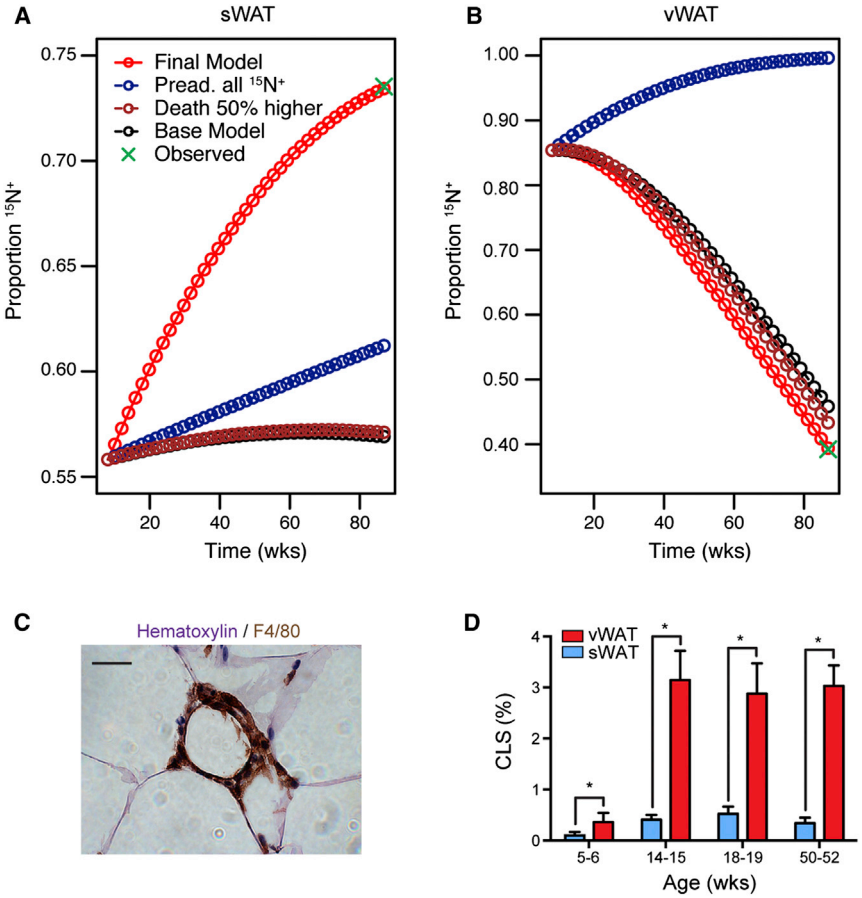

Figure 4. Modeling Adipocyte Turnover

(A) Simulated models of sWAT adipocyte turnover. Increasing the adipocyte death rate (Death 50% higher) did not substantially improve the fit of the model. Even an assumption of 100% progenitor ^{15}N-labeling at conclusion of pulse was insufficient to simulate the observed data. The data were best fit by the inclusion of progenitor differentiation without further division (Final Model).

(B) Modeling of vWAT adipocyte turnover.

(C) Representative "crown-like structure." F4/80 staining macrophages surrounding a necrotic adipocyte. Scale bar represents 20 μm.

(D) Relative frequencies of "crown-like structures" in the sWAT and vWAT of C57BL/6 mice as a function of age (mean ± SEM; n = 3–7).

See also Figure S6, Table S1, and Supplemental Experimental Procedures.

Model," Figures 4A and 4B). Finally, combining differentiation without division and a preadipocyte ^{15}N^{+} underestimation rate that varied between sWAT and vWAT, produced a set of assumptions that was able to simulate the full 17% label enrichment in sWAT while maintaining label dilution in the vWAT ("Final Model," Figures 4A and 4B; Table S1).

The final model of adipocyte turnover also predicts a depot difference in adipocyte death. We tested this prediction by a blinded histologic analysis of dead adipocytes, which are identifiable due to the characteristic influx of macrophages that surround the dead adipocyte, forming so-called "crown-like structures" (Murano et al., 2008) (Figure 4C). CLS were detected at higher frequencies in vWAT (Figure 4D), and the relative ratio between vWAT and sWAT CLS frequencies in the adult was consistent with adipocyte death as predicted by the model (Figure 4D; Table S1). Such empiric measurements of adipocyte death cannot be directly translated into a time-dependent death rate because the precise time to CLS clearance is unknown. However, these data are supportive of the "Final Model" in which adipocyte death is matched to adipocyte birth, the rate of which is due to progenitor differentiation, with and without preceding progenitor division.

Obesity-Related Adipocyte Hyperplasia Declines in the Adult

With limited sWAT plasticity during normal aging, what occurs with obesity? We first addressed this question in the diet-induced obesity model. C57BL/6 mice were randomly assigned to high-fat diet or control chow at 4 or 10 weeks of age, administered ^{15}N-thymidine pulse-chase, and followed by IRMS analysis of the adipocyte fractions. In 4-week-old mice, 5 weeks of high-fat feeding was associated with increased ^{15}N-labeling in both sWAT and vWAT adipocytes, consistent with increased adipogenesis (Figure 5A). A similar increase was not observed in adult mice, aged 10 weeks at study start. In a separate experiment, where a subset of 10-week-old mice were exposed to an 8 week run-in period of high-fat feeding, prior to 4 weeks of ^{15}N-thymidine labeling, a 57% increase ($p < 0.05$) in ^{15}N-labeling was observed in adipocytes isolated from vWAT, but not from sWAT, suggesting some capacity for adipocyte hyperplasia in the visceral depot (Figure 5B).

We also tested for differences in proliferative activity in progenitor containing stromal vascular fractions. Mice received chow or high-fat diet for 8 weeks followed by ^{15}N-thymidine for 1 week. IRMS analysis of unsorted stromal vascular cells or those subjected to either negative selection (excluding lineage^{+} and CD31^{+} endothelial cells) or positive selection for PDGFRα-expressing cells (Berry and Rodeheffer, 2013), generally showed increased proliferative activity in vWAT compared to sWAT (Figure 5C). High-fat feeding had a modest effect on ^{15}N-labeling in sWAT, only reaching statistical significance in the unsorted population. However, a robust increase in ^{15}N-signal was detected the PDGFRα^{+} fraction of vWAT after high-fat feeding. Because the stromal vascular cell fraction is comprised of a heterogeneous array of cell types, including endothelial cells, fibroblasts, macrophages, and progenitors, these analyses must be interpreted with caution, but taken together the results are largely consistent with concept that vWAT has a higher turnover rate than sWAT.

We also performed an evaluation of adipogenesis in a more extreme model of obesity, the *Lepr^{db}/Lepr^{db}* (db/db) mouse. Mice received a 2 week pulse of ^{15}N-thymidine followed by a

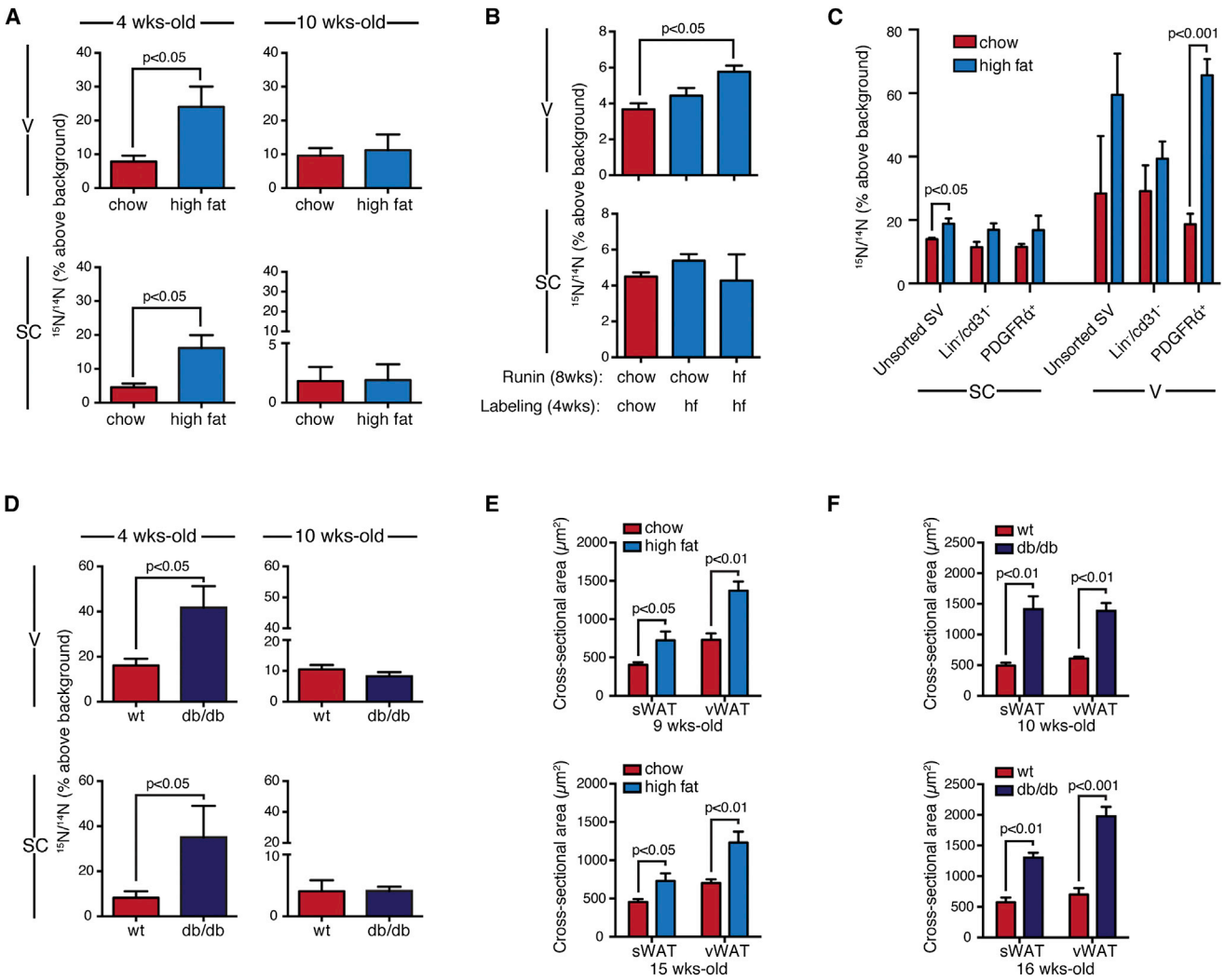

Figure 5. Obesity-Associated Adipose Tissue Plasticity Is Lost in the Adult

(A) Diet-induced obesity. Four-week-old mice showed increased ^{15}N-labeling of adipocytes with high-fat diet (mean ± SEM; n = 7–8 mice per group; $p < 0.05$). No difference was seen in 10-week-old mice, studied in parallel. ^{15}N-thymidine pulse for 2 weeks, followed by 3 week chase.

(B) An 8 week high-fat run-in increased ^{15}N-labeling of visceral, but not subcutaneous, adipocytes (mean ± SEM; n = 3–7 mice/group).

(C) Proliferative activity of progenitor-containing stromal vascular fractions. Mice administered chow or high-fat diet for 8 weeks prior to ^{15}N-thymidine for 1 week. Data expressed as mean ± SEM; n = 3–4/group.

(D) Increased ^{15}N-labeling of adipocytes was observed in 4-week-old $Lepr^{db}/Lepr^{db}$ (db/db) mice compared to WT controls (mean ± SEM; n = 5–6 mice per group, $p < 0.05$). Significant differences were not observed in adults (10 weeks). ^{15}N-thymidine pulse for 2 weeks, followed by 4 week chase.

(E) Mean adipocyte size (±SEM) after high-fat feeding at the conclusion of the labeling experiment described in (A).

(F) Mean adipocyte size (±SEM) in db/db mice versus WT mice at the conclusion of the labeling experiment described in (D).

WAT fractions were analyzed by IRMS. Each replicate is from a single mouse depot. See also Figure S3.

4 week label-free chase. Compared to WT mice on the same background, 4-week-old db/db mice demonstrated significant increases in adipocyte labeling in both sWAT and vWAT, although this effect was lost in adult mice (Figure 5D). If the db/db mice emerged from postnatal development with more adipocytes, as predicted by the higher level of labeling in the young mice, then the same relative rate of turnover (and therefore relative level of ^{15}N-labeling) would equal a higher absolute rate of adipogenesis. This observation is also consistent with predictions from a model of human adipocyte turnover, where obesity that was initiated prior to adulthood resulted in a higher number of adipocytes, a higher absolute rate of new adipocyte formation, but similar rates of relative turnover (Spalding et al., 2008).

Given the process entailed in isolating and purifying adipocytes from the heterogenous stromal vascular cells, it is important to consider possible sources of bias arising from an impure adipocyte preparation or the preferential loss of large adipocytes. Larger adipocytes are presumably older and unlabeled and therefore their selective loss during isolation would result in a falsely elevated ^{15}N/^{14}N ratio. Because obesity leads to increased proliferation of stromal-vascular elements, including infiltrating inflammatory cells, the contamination of the adipocyte

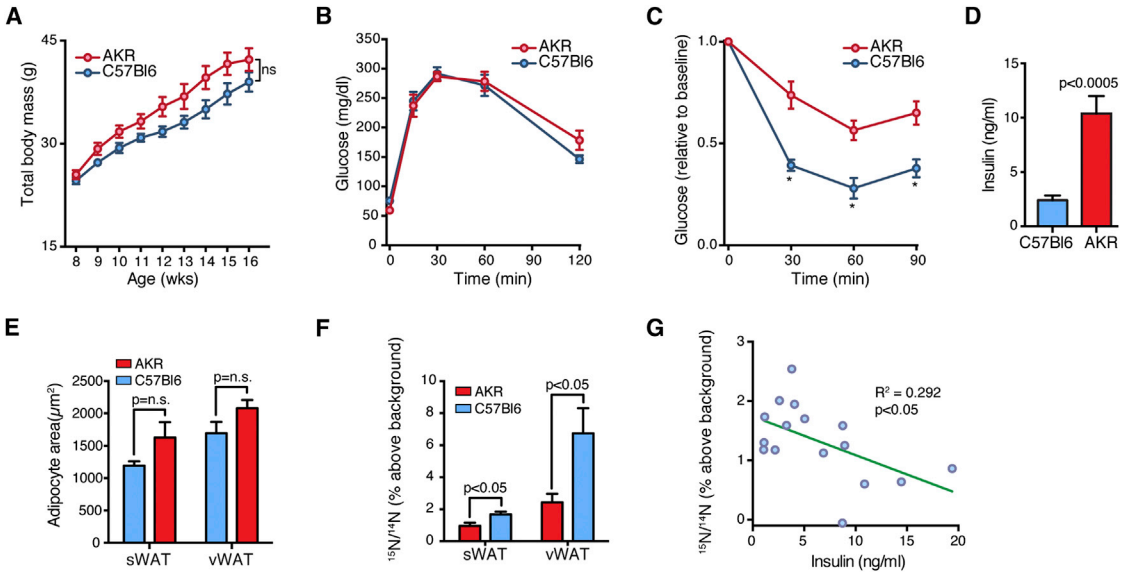

Figure 6. Impaired Adipocyte Turnover Is Associated with Insulin Resistance

(A) Weight gain during 8 weeks of high-fat feeding of C57BL/6 and AKR mice. Data expressed as mean ± SEM.

(B) Intraperitoneal (1.5 g/kg) glucose tolerance testing. Data expressed as mean ± SEM.

(C) Intraperitoneal (0.75 U/kg) insulin tolerance testing shows heightened insulin resistance in AKR mice relative to C57BL/6 mice. Data expressed as mean ± SEM, *$p < 0.05$.

(D) Mean serum insulin (±SEM) levels are higher in AKR mice, consistent with insulin resistance.

(E) Bar graph showing mean adipocyte cross-sectional area (±SEM) in C57BL/6 and AKR mice after 8.5 weeks high-fat feeding (n = 8 mice/strain).

(F) ^{15}N-labeling shows higher indices of adipogenesis in C57BL/6 mice compared to AKR mice. Data expressed as mean ± SEM.

(G) Negative correlation between sWAT ^{15}N-thymidine labeling of adipocytes and circulating insulin levels.

See also Figure S3.

fraction by proliferative stromal vascular cells would also cause a falsely elevated $^{15}N/^{14}N$ ratio. Therefore, both scenarios should lead to a false positive association between fat pad expansion and adipogenesis, not the flat response observed in the adult. Nonetheless, due to these potential sources of bias and given the observed interanimal variance in ^{15}N-labeling, we cannot exclude small differences in adipocyte turnover in the adult obesity models. However, taken together with the association between obesigenic stimuli and increased adipocyte size (Figures 5E and 5F), we conclude that adipocyte hypertrophy is the dominant mechanism of fat mass expansion in adult obesity.

sWAT Adipocyte Turnover Predicts Insulin Sensitivity with Obesity

A number of studies in animal models and humans have found adipocyte hypertrophy to predict metabolic disease (Kabir et al., 2011; Weyer et al., 2000), whereas a cross-sectional human study suggests that a hyperplastic tendency is predictive of metabolic health (Arner et al., 2010). In the absence of a strong association between adipocyte birth and fat mass expansion in the adult, we hypothesized that adipocyte turnover is metabolically beneficial. To test this, we applied quantitative stable isotope methodology to measure adipogenesis in two obesigenic mouse strains previously found to have different metabolic profiles, the C57BL/6 and AKR mice (Rossmeisl et al., 2003).

Adult male mice of both strains (n = 8) were started on a high-fat diet at 8 weeks of age. Mice underwent ^{15}N-thymidine labeling starting 4 weeks into high-fat feeding and metabolic parameters were assessed after a total of 8 weeks on the high-fat diet. Both strains gained a significant and similar amount of weight (Figure 6A). Although the C57BL/6 mice had higher serum glucose levels after an overnight fast (C57BL/6 = 75.6 ± 3.1 mg/dl, AKR = 59.4 ± 4.7 mg/dl, $p < 0.05$), the response to a 1 g/kg intraperitoneal glucose tolerance test was similar between the two strains (Figure 6B). In contrast, the AKR mice demonstrated more severe insulin resistance, both on the basis of a blunted response to an intraperitoneal insulin tolerance test (0.75 U/kg) and significantly higher serum insulin levels at the time of sacrifice (Figures 6C and 6D).

Although both strains showed a similar pattern of weight gain on a high-fat diet, there was a trend toward larger adipocytes in AKR mice (Figure 6E, sWAT p = 0.1, vWAT p = 0.1). Conversely, an IRMS analysis demonstrated significantly higher ^{15}N-labeling of both visceral and subcutaneous adipocytes from C57BL/6 mice compared to AKR mice, consistent with an increased rate of adipogenesis (Figure 6F) and a linear regression analysis showed an inverse association between sWAT adipogenesis (^{15}N labeling) and serum insulin levels (Figure 6G). Together, these data support the concept that a failure of adipose tissue plasticity is associated with insulin resistance.

DISCUSSION

The adipocyte is increasingly recognized as a regulator of energy balance, systemic metabolism, and inflammation (Cristancho and Lazar, 2011). Despite the intuitive appeal of targeting

adipocytes as a pathologic component of obesity, a number of often-cited observations support the concept that a dynamic adipocyte pool may be beneficial in states of excess energy consumption. Stimulation of PPARγ-dependent adipogenesis with thiazolidinedione drugs, for example, is associated with an insulin sensitizing effect, although distinguishing the specific effects of PPARγ activation responsible for this beneficial property is an area of active research (Choi et al., 2010). Conversely, impaired adipocyte development is associated with insulin resistance in a number of circumstances. For example, both mice and humans with lipodystrophy demonstrate severe insulin resistance (Moitra et al., 1998; Pajvani et al., 2005; Seip, 1959). Therefore, an open question is whether adipogenesis is an adaptive or maladaptive response in obesity.

Here, we developed a stable isotope approach to track adipogenesis, guided by the rationale that testing for associations between adipogenesis and obesity will lend insight into the contribution of fat cell development to disease pathogenesis. We show a marked age-dependent decline in homeostatic and obesity-related adipocyte plasticity. These data largely converge with older studies (Greenwood and Hirsch, 1974; Salans et al., 1971) and more recent ^{14}C birth dating (Spalding et al., 2008) in showing limited capacity for dynamic changes in adipocyte number in adults. We speculate that studies reporting substantially higher rates of adipocyte birth may reflect the challenge of distinguishing slowly dividing cell populations, such as adipocytes, from surrounding stromal-vascular cells that divide at higher rates (Klyde and Hirsch, 1979). We propose that this study is less prone to such bias due to the superior imaging resolution of MIMS and the quantitative precision of stable isotope methodology.

Our data point to a mechanism for limited plasticity of adipose tissue, the phenomenon of progenitor differentiation without preceding division (Figures 3 and 4). Without the stem cell property of self-renewal—or the clonal expansion step that precedes terminal differentiation in preadipocyte cell lines—the adipocyte progenitor pool may be programmed for exhaustion. If future studies confirm this phenomenon, it could represent an important mechanism of adipose tissue aging and functional decline with obesity. Moreover, with an inverse association between sWAT adipocyte turnover and insulin resistance, the intrinsic capacity for progenitor self-renewal represents an additional link between local adipose tissue function and systemic metabolism (Cohen et al., 2014; Tran et al., 2008).

An important question raised by these data then is whether there are any contexts in which adult WAT becomes hyperplastic. Indeed, this study does not exclude the possibility that adipogenesis is dynamically regulated in contexts outside of the standard obesity models used here, which were conducted with male mice. Given apparent gender differences in adiposity and propensity for adipocyte hypertrophy (Drolet et al., 2008; Lemieux et al., 1993), for example, sex may represent an important determinant of adipocyte progenitor function and WAT hyperplastic potential. In addition, the close association of adipocyte birth and death (Figure 4), also predicted from human modeling (Spalding et al., 2008), raises the possibility that an increase in adipocyte death would result in increased adipocyte birth. Interestingly, the one condition in the adult where we observed a modest, yet statistically significant, increase in adipogenesis was in the visceral depot after prolonged high-fat feeding (Figure 5), a condition also known to be associated with increased adipocyte death (Alkhouri et al., 2010). Moreover, a robust example of induced de novo adipocyte birth in the adult mouse occurs in response to widespread, programmed adipocyte apoptosis (Pajvani et al., 2005); therefore we speculate that adipocyte death is a causal determinant of adipogenesis.

From a methodological standpoint, it is important that our results demonstrate limited WAT plasticity, similar to studies using genetic lineage tracing (Wang et al., 2013) or ^{14}C-birthdating (Spalding et al., 2008). The relative agreement of these approaches suggests that they can be considered complementary tools to study adipocyte turnover. We anticipate that this study will provide a valuable template for future in vivo studies of adipogenesis, in large part due to the flexibility conferred by stable isotope tracers and their easy applicability to a wide-range of experimental models, including genetic models displaying obesity or metabolic phenotypes. Perhaps most important is the possibility of conducting prospective studies in humans, due to the extensive precedent of safe application of stable isotope methodology in human studies (Steinhauser and Lechene, 2013).

This study demonstrates that lack of adipogenesis, as opposed to adipogenesis, may be the maladaptive contributor to obesity-related diabetes mellitus. This is consistent with the intriguing hypothesis that diabetes mellitus arises from a failure of WAT plasticity (Heilbronn et al., 2004; McLaughlin et al., 2007; Pasarica et al., 2009; Wang et al., 2013). Therefore, this study provides additional rationale to test whether limitations in WAT progenitor self-renewal and differentiation are causally linked to obesity-related diseases.

EXPERIMENTAL PROCEDURES

Mouse Studies

Experiments were approved by the Harvard Medical Area Standing Committee on Animals. Male C57Bl/6 mice were purchased from Charles River. Male *Lepr^{db}/Lepr^{db}* mice and male WTs of the same background (C57BLKS/J) were purchased from Jackson Laboratories. Male AKR mice were purchased from Jackson Laboratories. Mice were housed at 22°C ± 2°C, with a 12 hr light (0700–1900 hr), 12 hr dark (1900–0700 hr) cycle and free access to food and water. Aging studies and those using *Lepr^{db}/Lepr^{db}* mice were conducted with a diet containing 23% protein, 21% fat, and 55% carbohydrates (PicoLab Mouse Diet 20). Diet-induced obesity was modeled with high fat (D12492) and control chow (D12450J) matched for sucrose content (Research Diets). Insulin tolerance tests were performed by injecting 0.75 U/kg regular insulin intraperitoneally (i.p.) after 4 hr of fasting. Glucose tolerance tests were performed by i.p. injection of glucose (1 g/kg) after an overnight fast. Blood was collected from the tail vein and measured by glucometer (Contour, Bayer). Serum was collected at the time of sacrifice and insulin measured by ELISA (Millipore).

Stable Isotopes

^{15}N-thymidine (Cambridge Isotope Laboratories) was dissolved in water (20 mg/ml). Prior to 4 weeks, mice were administered 50 μg/g/dose by subcutaneous injection (Hamilton syringe, 31 g needle) every 12 hr. For long-term labeling studies, mice 4 weeks or older were implanted with subcutaneous osmotic minipumps (Alzet), delivering 20 μg/hr continuously. For shorter term labeling studies in DIO or db/db mice, ^{15}N-thymidine was administered by subcutaneous injection (25 μg/g) every 12 hr.

MIMS

MIMS was performed as previously described (Steinhauser et al., 2012) using the prototype instrument and the NanoSIMS 50L (Cameca). Tissue was fixed

(4% paraformaldehyde), embedded in LR white, sectioned (0.5 μm), and mounted on silicon chips. Samples were analyzed in automated chain analysis mode, with each tile acquired at 256 × 256 pixels, 60 μm × 60 μm field size. Nuclei were manually traced in a customized plugin to ImageJ (OpenMIMS: http://nrims.harvard.edu/software) and assigned an identity of adipocyte, stromal-vascular cell, or possible adipocyte by an observer unaware of fat depot, experimental group, or labeling status of the cell. Typical reasons for the designation of "possible adipocyte" included imaging artifact (e.g., nucleus found at the margin of two adjacent fields) or inability to clearly distinguish a close association with a lipid droplet and shared plasma membrane. In these cases, the specific cell was reimaged at higher resolution (512 × 512 pixels, 10–25 μm raster size) and the images reevaluated by a blinded observer. Cross-sectional area was calculated by tracing the adipocyte periphery in ImageJ.

IRMS

Adipose tissue was minced and digested with collagenase type D (Roche) in a shaking water bath (37°C, 225 rpm, 40 min). The digest was filtered (300 μm nylon mesh, Spectrum Labs) and centrifuged at 400 × *g* for 10 min. Adipocytes were collected and washed two times with PBS. Pelleted stromal vascular cells were strained (40 μm) and then washed with PBS. For analyses of stromal-vascular subfractions, cells were subjected to additional positive (PDGFRα+) or negative selection (lineage$^-$) using antibody-coated microbeads (Miltenyi Biotec). Cells were aliquoted into tin cups and dried at 60°C. For analyses of genomic DNA, cells were directly lysed in DNAzole (MRC). Because of the possibility of finding small (<300 μm) incompletely digested tissue fragments containing stromal vascular cells adherent to buoyant adipocytes floating in the supranatant, analysis of aliquots of DAPI-stained adipocytes served as a quality control metric. This analysis reproducibly yielded an adipocyte preparation with minimal contamination from adherent nonadipocytes (≈98%). Samples were introduced to an elemental analyzer (Vario Pyrocube, Elementar) coupled to an IRMS (Isoprime 100, Elementar). Tuning was confirmed with urea standards. Samples obtained from unlabeled mice were used as the natural background. Data were expressed as % above natural ratio, a value obtained by the following equation: 100 × (Sample – Control)/0.37.

Histology

Adipose tissue specimens were fixed with 4% paraformaldehyde, paraffin-embedded, sectioned, and stained using standard methods. Cross-sectional areas of adipocytes in hematoxylin and eosin (H&E)-stained sections were calculated by tracing the adipocyte periphery in ImageJ by a blinded observer. For immunohistochemistry, an antigen retrieval step was used by heating samples in a citrate-based buffer (Dako) at 95°C for 20 min. A rat monoclonal primary antibody to murine F4/80 (Abcam) was used at a concentration of 1:250 for 1 hr at room temperature. Endogenous peroxidase activity was quenched with a 20 min incubation in 0.3% H_2O_2. A mouse adsorbed and biotinylated goat anti-rat IgG secondary antibody was used at a concentration of 1:250 for 1 hr, followed by ABC reagent and DAB (Vector Laboratories). "Crown like structures" were identified and counted by an observer, blinded to depot and experimental group.

Statistics

Statistical analyses were performed with Jmp10.0 and Prism 6.0. The Student's t test was used to compare two, independent, normally distributed groups and the Mann-Whitney test used when one or more groups did not pass a Shapiro-Wilk normality test. The Kruskal-Wallis test was used to compare non-normally distributed data involving multiple groups, with significance assigned for $\alpha < 0.05$ after a Dunn's multiple comparison correction. Proportions were compared using the χ^2 test. A p value < 0.05 on a two-tailed test was used to indicate significance.

SUPPLEMENTAL INFORMATION

Supplemental Information includes Supplemental Experimental Procedures, six figures, one table, and three data files and can be found with this article online at http://dx.doi.org/10.1016/j.cmet.2014.10.010.

AUTHOR CONTRIBUTIONS

S.M.K. performed animal experiments, tissue fractionation, and histology. M.L. performed histology and insulin measurements. M.W. and C.G. operated NanoSIMS instruments. S.E.S. assisted with mouse experiments and helped develop the IRMS approach. P.P. developed the modeling, wrote the code for all simulations, analyzed the modeling data, and assisted with writing the manuscript. M.L.S. designed the study, performed animal experiments, performed histology, performed IRMS measurements, analyzed the data, and wrote the manuscript. All authors approved the manuscript.

ACKNOWLEDGMENTS

We thank C. Lechene for critical feedback and the National Resource for Imaging Mass Spectrometry where NanoSIMS analyses were conducted. We thank R. Lee for critical feedback. We thank P. Cohen, J. Brown, and W. Chutkow for critical evaluation of the manuscript. S.E.S is funded by the NIH (HL108570). M.L.S. is funded by the Harvard Stem Cell Institute, the Brigham and Women's Hospital Watkins Cardiovascular Leadership Award, and the NIH (DK090147).

Received: May 22, 2014
Revised: September 10, 2014
Accepted: October 15, 2014
Published: November 20, 2014

REFERENCES

Alkhouri, N., Gornicka, A., Berk, M.P., Thapaliya, S., Dixon, L.J., Kashyap, S., Schauer, P.R., and Feldstein, A.E. (2010). Adipocyte apoptosis, a link between obesity, insulin resistance, and hepatic steatosis. J. Biol. Chem. *285*, 3428–3438.

Arner, E., Westermark, P.O., Spalding, K.L., Britton, T., Rydén, M., Frisén, J., Bernard, S., and Arner, P. (2010). Adipocyte turnover: relevance to human adipose tissue morphology. Diabetes *59*, 105–109.

Berry, R., and Rodeheffer, M.S. (2013). Characterization of the adipocyte cellular lineage in vivo. Nat. Cell Biol. *15*, 302–308.

Choi, J.H., Banks, A.S., Estall, J.L., Kajimura, S., Boström, P., Laznik, D., Ruas, J.L., Chalmers, M.J., Kamenecka, T.M., Blüher, M., et al. (2010). Anti-diabetic drugs inhibit obesity-linked phosphorylation of PPARgamma by Cdk5. Nature *466*, 451–456.

Cohen, P., Levy, J.D., Zhang, Y., Frontini, A., Kolodin, D.P., Svensson, K.J., Lo, J.C., Zeng, X., Ye, L., Khandekar, M.J., et al. (2014). Ablation of PRDM16 and beige adipose causes metabolic dysfunction and a subcutaneous to visceral fat switch. Cell *156*, 304–316.

Cristancho, A.G., and Lazar, M.A. (2011). Forming functional fat: a growing understanding of adipocyte differentiation. Nat. Rev. Mol. Cell Biol. *12*, 722–734.

Drolet, R., Richard, C., Sniderman, A.D., Mailloux, J., Fortier, M., Huot, C., Rhéaume, C., and Tchernof, A. (2008). Hypertrophy and hyperplasia of abdominal adipose tissues in women. Int. J. Obes. (Lond.) *32*, 283–291.

Ellis, J.R., McDonald, R.B., and Stern, J.S. (1990). A diet high in fat stimulates adipocyte proliferation in older (22 month) rats. Exp. Gerontol. *25*, 141–148.

Greenwood, M.R., and Hirsch, J. (1974). Postnatal development of adipocyte cellularity in the normal rat. J. Lipid Res. *15*, 474–483.

Gupta, R.K., Mepani, R.J., Kleiner, S., Lo, J.C., Khandekar, M.J., Cohen, P., Frontini, A., Bhowmick, D.C., Ye, L., Cinti, S., and Spiegelman, B.M. (2012). Zfp423 expression identifies committed preadipocytes and localizes to adipose endothelial and perivascular cells. Cell Metab. *15*, 230–239.

Heilbronn, L., Smith, S.R., and Ravussin, E. (2004). Failure of fat cell proliferation, mitochondrial function and fat oxidation results in ectopic fat storage, insulin resistance and type II diabetes mellitus. Int. J. Obes. Relat. Metab. Disord. *28* (*Suppl 4*), S12–S21.

Hood, R.L., and Allen, C.E. (1977). Cellularity of porcine adipose tissue: effects of growth and adiposity. J. Lipid Res. *18*, 275–284.

Jo, J., Gavrilova, O., Pack, S., Jou, W., Mullen, S., Sumner, A.E., Cushman, S.W., and Periwal, V. (2009). Hypertrophy and/or Hyperplasia: Dynamics of Adipose Tissue Growth. PLoS Comput. Biol. *5*, e1000324.

Jo, J., Guo, J., Liu, T., Mullen, S., Hall, K.D., Cushman, S.W., and Periwal, V. (2010). Hypertrophy-driven adipocyte death overwhelms recruitment under prolonged weight gain. Biophys. J. *99*, 3535–3544.

Johnson, P.R., Stern, J.S., Greenwood, M.R., and Hirsch, J. (1978). Adipose tissue hyperplasia and hyperinsulinemia on Zucker obese female rats: a developmental study. Metabolism *27* (12, Suppl 2), 1941–1954.

Kabir, M., Stefanovski, D., Hsu, I.R., Iyer, M., Woolcott, O.O., Zheng, D., Catalano, K.J., Chiu, J.D., Kim, S.P., Harrison, L.N., et al. (2011). Large size cells in the visceral adipose depot predict insulin resistance in the canine model. Obesity (Silver Spring) *19*, 2121–2129.

Klyde, B.J., and Hirsch, J. (1979). Isotopic labeling of DNA in rat adipose tissue: evidence for proliferating cells associated with mature adipocytes. J. Lipid Res. *20*, 691–704.

Lechene, C., Hillion, F., McMahon, G., Benson, D., Kleinfeld, A.M., Kampf, J.P., Distel, D., Luyten, Y., Bonventre, J., Hentschel, D., et al. (2006). High-resolution quantitative imaging of mammalian and bacterial cells using stable isotope mass spectrometry. J. Biol. *5*, 20.

Lemieux, S., Prud'homme, D., Bouchard, C., Tremblay, A., and Després, J.P. (1993). Sex differences in the relation of visceral adipose tissue accumulation to total body fatness. Am. J. Clin. Nutr. *58*, 463–467.

Lemonnier, D. (1972). Effect of age, sex, and sites on the cellularity of the adipose tissue in mice and rats rendered obese by a high-fat diet. J. Clin. Invest. *51*, 2907–2915.

McLaughlin, T., Sherman, A., Tsao, P., Gonzalez, O., Yee, G., Lamendola, C., Reaven, G.M., and Cushman, S.W. (2007). Enhanced proportion of small adipose cells in insulin-resistant vs insulin-sensitive obese individuals implicates impaired adipogenesis. Diabetologia *50*, 1707–1715.

Moitra, J., Mason, M.M., Olive, M., Krylov, D., Gavrilova, O., Marcus-Samuels, B., Feigenbaum, L., Lee, E., Aoyama, T., Eckhaus, M., et al. (1998). Life without white fat: a transgenic mouse. Genes Dev. *12*, 3168–3181.

Murano, I., Barbatelli, G., Parisani, V., Latini, C., Muzzonigro, G., Castellucci, M., and Cinti, S. (2008). Dead adipocytes, detected as crown-like structures, are prevalent in visceral fat depots of genetically obese mice. J. Lipid Res. *49*, 1562–1568.

Neese, R.A., Misell, L.M., Turner, S., Chu, A., Kim, J., Cesar, D., Hoh, R., Antelo, F., Strawford, A., McCune, J.M., et al. (2002). Measurement in vivo of proliferation rates of slow turnover cells by 2H2O labeling of the deoxyribose moiety of DNA. Proc. Natl. Acad. Sci. USA *99*, 15345–15350.

Pajvani, U.B., Trujillo, M.E., Combs, T.P., Iyengar, P., Jelicks, L., Roth, K.A., Kitsis, R.N., and Scherer, P.E. (2005). Fat apoptosis through targeted activation of caspase 8: a new mouse model of inducible and reversible lipoatrophy. Nat. Med. *11*, 797–803.

Pasarica, M., Xie, H., Hymel, D., Bray, G., Greenway, F., Ravussin, E., and Smith, S.R. (2009). Lower total adipocyte number but no evidence for small adipocyte depletion in patients with type 2 diabetes. Diabetes Care *32*, 900–902.

Rigamonti, A., Brennand, K., Lau, F., and Cowan, C.A. (2011). Rapid cellular turnover in adipose tissue. PLoS ONE *6*, e17637.

Rodeheffer, M.S., Birsoy, K., and Friedman, J.M. (2008). Identification of white adipocyte progenitor cells in vivo. Cell *135*, 240–249.

Rossmeisl, M., Rim, J.S., Koza, R.A., and Kozak, L.P. (2003). Variation in type 2 diabetes—related traits in mouse strains susceptible to diet-induced obesity. Diabetes *52*, 1958–1966.

Salans, L.B., Horton, E.S., and Sims, E.A. (1971). Experimental obesity in man: cellular character of the adipose tissue. J. Clin. Invest. *50*, 1005–1011.

Salans, L.B., Cushman, S.W., and Weismann, R.E. (1973). Studies of human adipose tissue. Adipose cell size and number in nonobese and obese patients. J. Clin. Invest. *52*, 929–941.

Seip, M. (1959). Lipodystrophy and gigantism with associated endocrine manifestations. A new diencephalic syndrome? Acta Paediatr. *48*, 555–574.

Senyo, S.E., Steinhauser, M.L., Pizzimenti, C.L., Yang, V.K., Cai, L., Wang, M., Wu, T.D., Guerquin-Kern, J.L., Lechene, C.P., and Lee, R.T. (2013). Mammalian heart renewal by pre-existing cardiomyocytes. Nature *493*, 433–436.

Spalding, K.L., Arner, E., Westermark, P.O., Bernard, S., Buchholz, B.A., Bergmann, O., Blomqvist, L., Hoffstedt, J., Näslund, E., Britton, T., et al. (2008). Dynamics of fat cell turnover in humans. Nature *453*, 783–787.

Steinhauser, M.L., and Lechene, C.P. (2013). Quantitative imaging of subcellular metabolism with stable isotopes and multi-isotope imaging mass spectrometry. Semin. Cell Dev. Biol. *24*, 661–667.

Steinhauser, M.L., Bailey, A.P., Senyo, S.E., Guillermier, C., Perlstein, T.S., Gould, A.P., Lee, R.T., and Lechene, C.P. (2012). Multi-isotope imaging mass spectrometry quantifies stem cell division and metabolism. Nature *481*, 516–519.

Stürup, S., Hansen, H.R., and Gammelgaard, B. (2008). Application of enriched stable isotopes as tracers in biological systems: a critical review. Anal. Bioanal. Chem. *390*, 541–554.

Tang, W., Zeve, D., Suh, J.M., Bosnakovski, D., Kyba, M., Hammer, R.E., Tallquist, M.D., and Graff, J.M. (2008). White fat progenitor cells reside in the adipose vasculature. Science *322*, 583–586.

Tang, W., Zeve, D., Seo, J., Jo, A.Y., and Graff, J.M. (2011). Thiazolidinediones regulate adipose lineage dynamics. Cell Metab. *14*, 116–122.

Tran, T.T., Yamamoto, Y., Gesta, S., and Kahn, C.R. (2008). Beneficial effects of subcutaneous fat transplantation on metabolism. Cell Metab. *7*, 410–420.

Wang, Q.A., Tao, C., Gupta, R.K., and Scherer, P.E. (2013). Tracking adipogenesis during white adipose tissue development, expansion and regeneration. Nat. Med. *19*, 1338–1344.

Weyer, C., Foley, J.E., Bogardus, C., Tataranni, P.A., and Pratley, R.E. (2000). Enlarged subcutaneous abdominal adipocyte size, but not obesity itself, predicts type II diabetes independent of insulin resistance. Diabetologia *43*, 1498–1506.

Cell Metabolism, Volume *20*

Supplemental Information

Loss of White Adipose Hyperplastic Potential Is Associated with Enhanced Susceptibility to Insulin Resistance

Soo M. Kim, Mingyue Lun, Mei Wang, Samuel E. Senyo, Christelle Guillermier, Parth Patwari, and Matthew L. Steinhauser

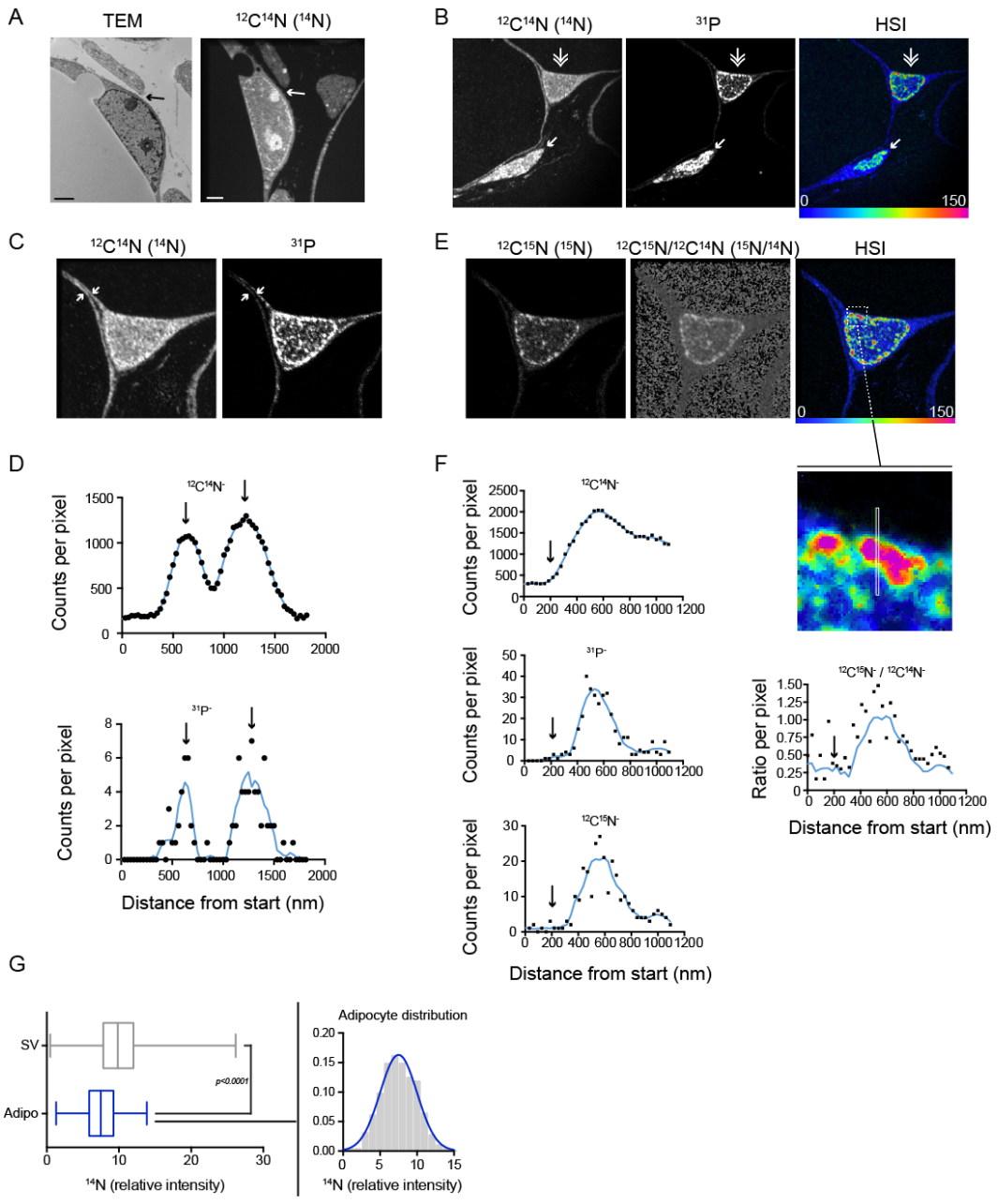

Figure S1 (related to Figure 1). Identifying adipocytes with multi-isotope imaging mass spectrometry (MIMS).

This study utilized qualitative and quantitative aspects of high-resolution MIMS images to distinguish adipocyte nuclei from surrounding interstitial cells. The assignment of adipocyte identify was conducted by a blinded observer. (A) Here, adjacent sections were imaged with transmission electron microscopy (left) and MIMS (right), showing qualitative similarities between

the two methods. The adipocyte nucleus is distinguishable by its close approximation to its defining lipid droplet both contained within the plasma membrane. The arrow shows a sub-micron space between the adipocyte nucleus and an adjacent cell structure in both the TEM image and MIMS image. Scale bar = 2 μm. (B) Shown is an example of an adipocyte nucleus that required additional imaging to verify its identity. The hatched arrow shows the candidate adipocyte nucleus. The small arrow shows a ^{15}N-thymidine labeled interstitial cell. (C) Higher resolution imaging of the adipocyte shown in "B". The white arrows show a region where the plasma membranes of two adjacent adipocytes abut each other. The two adjacent membranes are resolvable visually at this resolution, but can also be identified quantitatively (D) with a line profile taken from a region between the two white arrows. The two peaks (black arrows) correspond to the two adjacent membranes. The ability to rapidly show quantitative line profiles is a feature of the OpenMIMS software (see experimental procedures), which enabled its use in real time by the observer assigning cell identity. Top (D): shows counts of CN^- as a function of distance in nanometers. With this acquisition (512 x 512 pixels, field=16 x 16 μm), the dimensions of each pixel are 31.25 x 31.25 nm. The y-axis represents counts of CN^- ions/pixel. Because of the low ionization efficiency of native nitrogen atoms, nitrogen images are based on measuring CN^- ions. This is made possible by the high mass resolution of the instrument, which distinguishes $^{13}C^{14}N^-$ from $^{12}C^{15}N^-$. Bottom (D): shows the counts of P^-, which are at higher concentrations in phosphor-lipid membranes and the nucleus. (E) Left: Direct measurement of $^{12}C^{15}N^-$ (representative of ^{15}N) is the numerator in the ratio images to the right. The value of the HSI ratio image (far right) provides richer information compared to the grey-scale ratio image (middle), however the underlying quantitative data is not modified by changes in the gray or color scale. For the data collected for this study, the observer assigning adipocyte identity was blind to the data contained in the ratio images. (F) Quantitative line profiles show the close approximation of the lipid droplet (appearing black) to the ^{15}N-labeled nucleus. A region from the lipid droplet / nuclear interface shown in (E) is blown up. Quantitative line profiles are from the vertical white box that is one pixel wide. The inflection point (black arrow at ~ 200nm) in the $^{12}C^{14}N^-$ graph (top) represents the transition from the nitrogen poor droplet to the droplet / nuclear interface. In the same line profile,

there is a slight lag (~100nm) before the increase in P^- counts and increase in the $^{12}C^{15}N^-/^{12}C^{14}N^-$ ratio, consistent with ^{15}N-labeled chromatin. The statistical noise in the first 200nm of the ratio line profile is due to the low counting statistic in the nitrogen-poor lipid droplet. (G) Post-hoc quality control evaluation of the fidelity of adipocyte identification. Different cell types often display different intensities in the nuclear nitrogen signal, presumably due to different degrees of chromatin density and/or protein content. Therefore, the ^{14}N-intensity distribution of a heterogeneous cell population, such as the stromal-vascular fraction (SV) of adipose tissue, does not demonstrate a Gaussian distribution (n=2873). Nuclei identified as adipocytes (n=297), however, are significantly less ^{14}N-intense and segregate into a single Gaussian population shown on the right (Shapiro-Wilk test).

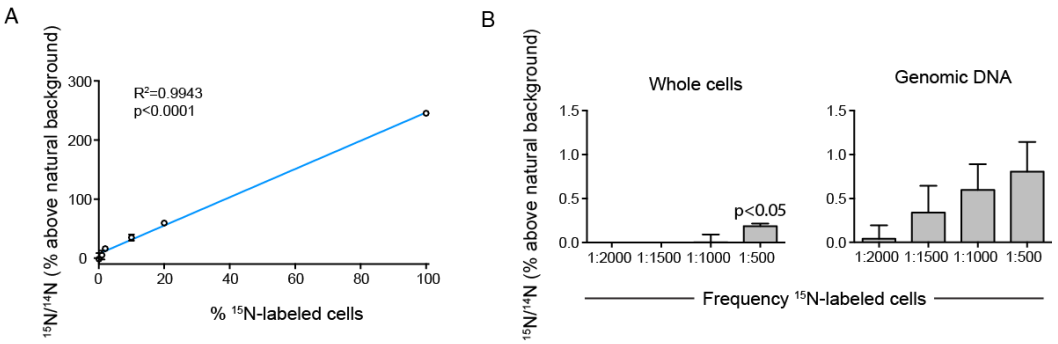

Figure S2 (related to Figure 1). Measuring ^{15}N-thymidine labeled cells with IRMS. 3T3L1 cells were cultured in ^{15}N-thymidine and then mixed at different ratios with unlabeled cells. (A) Linear relationship between ^{15}N-signal and % ^{15}N-labeled cells. (B) Detection of low frequency ^{15}N-labeling, comparing analysis of whole cells or genomic DNA. As expected isolation of genomic DNA strengthens the signal, but we generally observed increased variance of measurements, presumably due to the extra experimental step of genomic DNA isolation. Detection of whole labeled cells was possible down to about 1:500 frequency. Data expressed as mean, ± s.e.m.

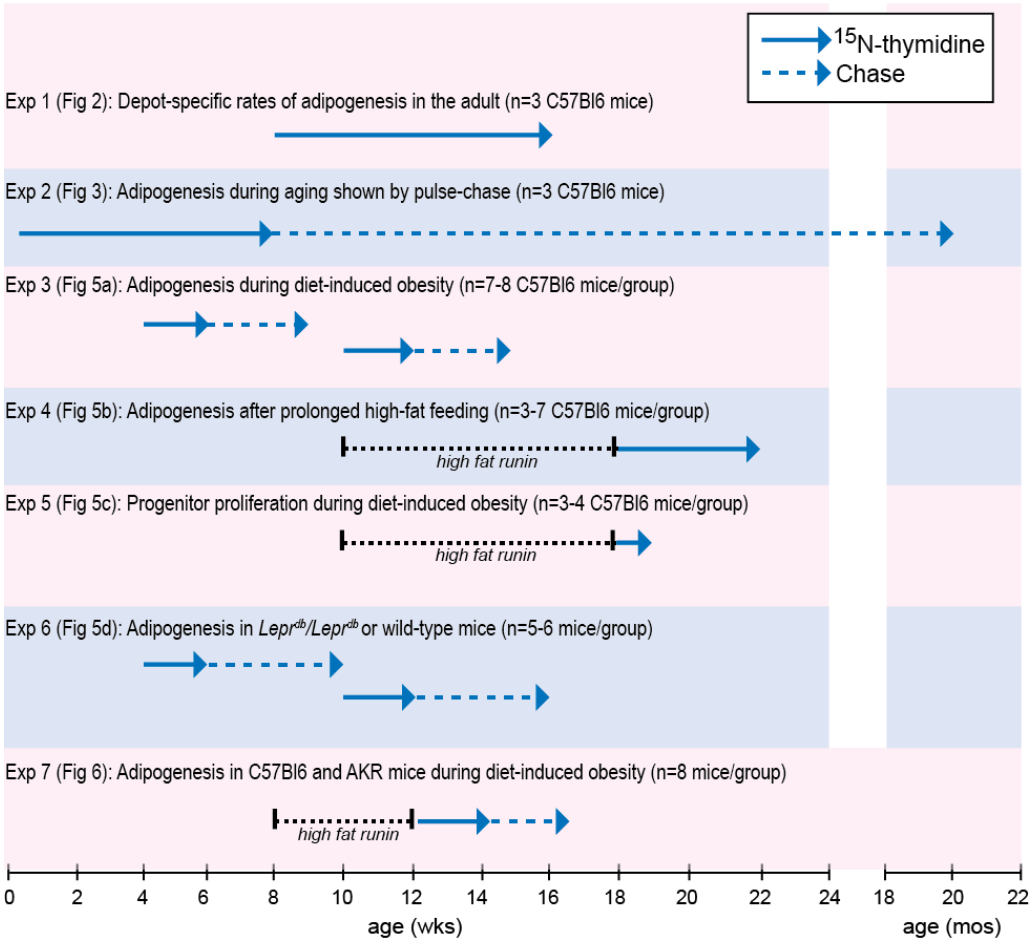

Figure S3 (related to Figures 2,3,5,6). Labeling protocols.

Experiment 1: ^{15}N-thymidine was administered for 8 wks to adult male C57Bl6 mice by osmotic minipump at a continuous rate of 20μg/h.

Experiment 2: ^{15}N-thymidine was administered from post-natal day 4 through week 4 by twice daily subcutaneous injection (50μg/g). At 4 wks, when the mice were large enough, osmotic minipumps were implanted to deliver a continuous rate of 20μg/h through week 8. Mice then underwent an 18-month label-free chase.

Experiment 3: Male C57Bl6 mice, aged 4 or 10 wks, were randomly assigned to normal chow or high fat diet, during ^{15}N-thymidine pulse-chase, which was administered by twice daily subcutaneous injection (25μg/g) for two wks, followed by 3wk label free chase.

Experiment 4: Male C57Bl6 mice, aged 10 wks underwent an 8 wk dietary run-in, receiving normal chow or high fat feeding. They then received ^{15}N-thymidine by osmotic minipump for 4 wks.

Experiment 5: Male C57Bl6 mice, aged 10 wks underwent an 8 wk dietary run-in, receiving normal chow or high fat feeding followed by one wk of ^{15}N-thymidine (25μg/g, twice daily).

Experiment 6: Male *Lepr^{db}/Lepr^{db}* on a C57Bl6SJ background or wild-type (C57Bl6SJ) mice, aged 4 or 10 wks, received ^{15}N-thymidine for 2 wks administered by twice daily subcutaneous injection (25μg/g), followed by 4wk label free chase.

Experiment 7: Male C57Bl6 or AKR mice (8 wks-old) received high fat feeding for 8.5 wks. ^{15}N-thymidine was delivered continuously starting at week 4 for 2 wks. Insulin and glucose tolerance testing was performed after the 8th wk of high fat feeding and the mice sacrificed at 8.5 wks.

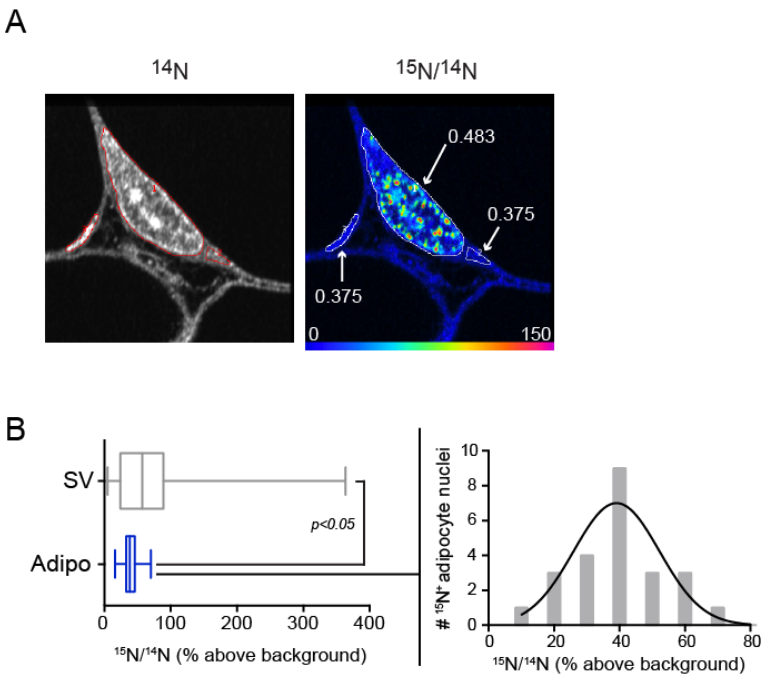

Figure S4 (related to Figure 2). A statistically distinct population of ^{15}N-labeled adipocytes is evident after 8 weeks of continuous ^{15}N-thymidine administration in the adult mouse. (A) Representative ^{15}N-thymidine labeled adipocyte (n= 24). Three regions of interest are shown with their corresponding ^{15}N/^{14}N ratio. Left: small ^{14}N-intense region representing the edge of a nucleus at natural background. Bottom right: region of cytoplasm at natural background. Middle: ^{15}N-labeled nucleus. The rainbow scale ranges from 0-150 % above natural background. (B) ^{15}N-labeled nuclei cluster in a single normally distributed population that is statistically distinct from the skewed distribution displayed by heterogeneous stromal vascular cells that are ^{15}N-thymidine labeled. Cell type specific differences in labeling intensity are likely due to differences in the density of chromatin within the nucleus and/or the result of cells undergoing more than one round of division during the labeling period.

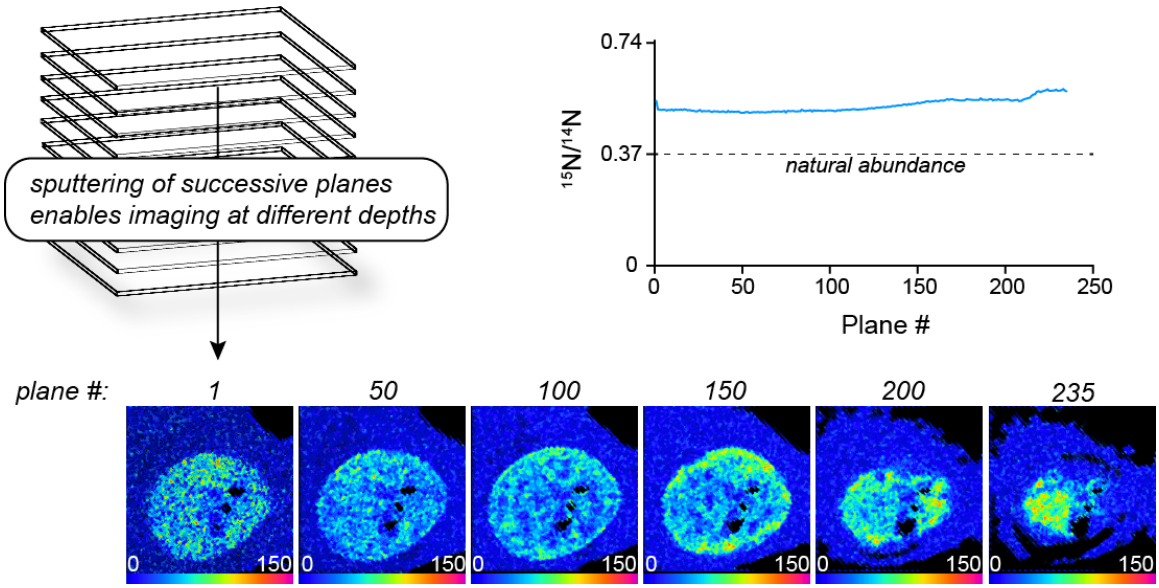

Figure S5 (related to Figure 3). Thin MIMS imaging planes provide a quantitative representation of whole nuclear labeling. 0.5 micron tissue sections were used in this study, but MIMS generates images from a sample volume with a depth dimension as low as a few atomic layers(Lechene et al., 2006; Steinhauser et al., 2012). Shown are representative analytical planes of a fibroblast cultured in ^{15}N-thymidine and subjected to successively deeper measurements. Top right: $^{15}N/^{14}N$ ratio as a function of depth (plane #). The isotope ratio remains quite constant, suggesting that sampling of any given plane provides a quantitative measure of total nuclear labeling, pertinent to quantitative analyses shown in Figure 3. More intense labeling is seen at the periphery of the nucleus, consistent with the tendency of chromatin to condense close to the nuclear membrane and accounting for the subtle increase in isotope ratio at the lower depths of the nucleus shown (between planes 200-235).

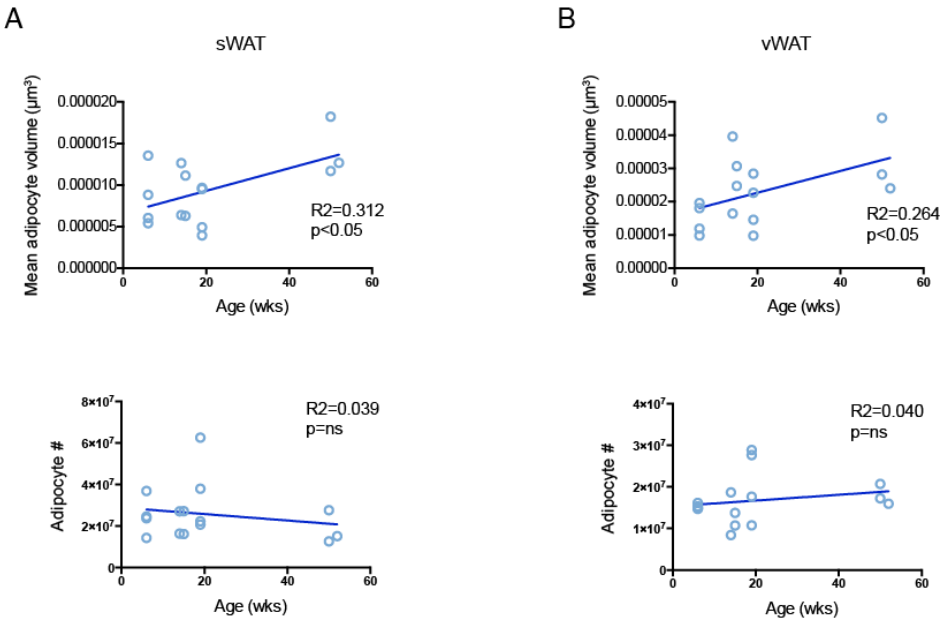

Figure S6 (related to Figure 4). Stability of adipocyte number in adult WAT. Adipocytes were tracked in serial sections. Individual adipocyte volumes were obtained by determining the maximal dimensions of individual adipocytes, using a modification to previously validated methods(Sjostrom et al., 1971). The maximum dimensions of each adipocyte were converted to a volume estimate, assuming sphericity. Total depot volume was calculated by measuring the volume of water displaced by submersion of the excised depot, measurements that as expected were highly correlated with depot mass (R^2=0.953, p<0.0001). Adipocyte number was then calculated by dividing the depot volume by its average adipocyte volume. (A) sWAT morphometrics. Top shows growth of adipocyte volume as a function of age. Bottom: shows no significant change in adipocyte number as a function of age. (B) vWAT morphometrics. Top shows growth of adipocyte volume as a function of age. Bottom: shows no significant change in adipocyte number as a function of age.

Table S1 (related to Figure 4)

	Adipocyte ^{15}N-Positive Proportion (%)		Death Rate (%/week)		Mean Adipocyte Age (weeks)	
	sWAT	**vWAT**	**sWAT**	**vWAT**	**sWAT**	**vWAT**
Actual outcome	73.5	39.2				
Baseline outcome	56.9 (55.4, 58.2)	45.9 (42.7, 48.8)	0.15	2.3	78.9 (78.7, 79.0)	26.9 (26.3, 27.5)
No cell death	56.7 (55.7, 57.6)	53.0 (52.0, 54.1)	0	0	79.1 (78.9, 79.2)	37.2 (37.2, 37.3)
Adipocyte death 50% higher	57.1 (55.5, 58.7)	43.3 (38.8, 48.0)	0.23	3.4	78.8 (78.6, 79.0)	23.6 (22.7, 24.5)
All pre-adipocytes $^{15}N^{+}$	61.2 (60.1, 62.2)	99.6 (99.2, 100.0)	0.15	2.3	78.9 (78.7, 79.0)	26.9 (26.3, 27.6)
Differentiation without division	60.2 (57.5, 62.9)	31.6 (28.7, 34.4)	0.95	7.2	53.2 (52.7, 53.7)	7.88 (7.67, 8.09)
Final model	73.4 (70.9, 75.8)	39.4 (36.6, 42.5)	0.95	3.3	53.2 (52.7, 53.7)	18.3 (17.8, 18.7)

Results of simulation for label-free chase from week 8 until 20 months of age. Results for ^{15}N-positive proportion and adipocyte age are presented as mean (95% confidence interval), calculated by bootstrapping.

Simulation Methods

Overview

We developed a simulation model which takes as input our quantitative experimental data and simulates at a single-cell level ^{15}N label state, birth, death, age, and size. In contrast to previous mathematical models, the extensive quantitative single-cell data allows stochastic simulation by random sampling of probability density functions estimated directly from the observed data. The model includes several parameters that allow testing multiple alternate hypotheses and determining the sensitivity of the outcome to multiple assumptions. All computations were performed in R (v. 3.01, The R Foundation for Statistical Computing, Vienna, Austria). Major methods and assumptions are described below; however, detailed methodology is described within the full source code in R, which is attached as a supplement.

Inputs and Initial Conditions

As input the model used the following observations:

i) SVC ^{15}N label proportions at the beginning and end of Chase
ii) Adipocyte ^{15}N label status and cross-sectional areas at the beginning of the Chase
iii) Adipocyte depot cell number and cell mass over time

Initial cell label proportions were set to the observed proportions for the respective depot at the beginning of the label-free chase. To simulate cell size, the observed cross-sectional areas at the end of the label pulse were used to estimate probability density functions describing cell area for labeled and unlabeled cells in the sWAT and the vWAT. For each simulation run, initial cell areas were then obtained by sampling from the appropriate density function.

Adipocyte Birth and Death

Adipocyte birth rate was given by the birth rate observed during the adult pulse experiment and was assumed to be constant over time. Whether each cell was ^{15}N-positive was determined randomly based on the proportion of ^{15}N-positive preadipocytes in the respective depot. Although the 15N label intensity in the SVC at the beginning of the label-free chase was directly observed, this population is heterogeneous and may underestimate the ^{15}N-positive rate in the progenitor cell population. We therefore included a parameter describing the underestimation rate in each depot. The proportion of labeled progenitor cells was also approximated as decreasing linearly with time over the course of the label-free chase.

Adipocyte cell death was determined stochastically at each time step, with the probability that a given cell dies proportional to the cell's cross-sectional area. The overall cell death rate was modeled as directly proportional the birth rate.

Differentiation without division

In the case that a population of previously labeled progenitor cells differentiate into mature adipocytes without accompanying renewal through division, the rate of ^{15}N-labeled cells observed during the adult pulse experiment will underestimate the overall adipocyte birth rate. We therefore develop an mathematical expression describing the underestimate for use in the model.

First we assume that the overall adipocyte birth rate is a constant, *g*. Then the rate of change of the total number of adipocytes *N* is given by:

$$\frac{dN}{dt} = g$$

So for t > 0, and N(t=0) = N_0, *N(t)* is given by:

$$N(t) = g\,t + N_0$$

However, the number of observed $^{15}N^+$ adipocytes immediately following a ^{15}N-thymidine pulse only gives *g* directly if all new adipocytes form by differentiation of dividing preadipocytes. If some new adipocytes form by differentiation of existing pre-adipocytes without further division, not all new adipocytes will be labeled $^{15}N^+$. The rate of formation of ^{15}N-negative adipocytes can be described as the product of the fraction of preadipocytes that are unlabeled, $f_{SVC-}(t)$, and the fraction of the overall adipocyte birth rate that proceeds by differentiation without division, f_{DS}. The rate of change of ^{15}N-positive cells is then:

$$\frac{dN_{15N+}}{dt} = g - f_{SVC-}(t)\,f_{DS}\,g$$

Modeling the increase in the labeled fraction of the SVC compartment as linear over time for the 8-week pulse, we let $f_{SVC+}(t) = at$, where $a = f_{SVC+}(t = 8\ wks)/8\ wks$. Then

$$\frac{dN_{15N+}}{dt} = (1 - f_{DS})\,g + f_{DS}\,a\,g\,t$$

Integration gives

$$N_{15N+} = (1 - f_{DS})\,g\,t + \frac{1}{2}a\,g\,t^2$$

Solving for the fraction of ^{15}N-positive adipocytes observed at t > 0 yields

$$\frac{N_{15N+}(t)}{N(t)} = \frac{(1 - f_{DS})\,g\,t + \frac{1}{2}(f_{DS})\,a\,g\,t^2}{g\,t + N_0}$$

Finally, solving for the true birth rate *g* based on the observed data at *t* = 8 weeks:

$$g = \frac{\frac{N_{15N+}(t=8)}{N(t=8)}}{8\left[(1 - f_{DS}) + \frac{1}{2}f_{DS}\,f_{SVC}(t=8)\right]}N_0$$

Model Output

The final mean adipocyte ^{15}N label proportion and adipocyte age were recorded directly from the simulation. Adipocyte lifetime over this time period was heavily censored, but was estimated by the average lifetime of cells that died at the end of the chase. 95% confidence intervals for the mean values were generated by bootstrapping from the simulation results.

Simulation Results

All reported results are for at least 1000 independent runs of 1000 cells in each depot simulated over 18 months in 40 time steps. Increasing these numbers further had little effect on the model results and confidence intervals.

The results of the final model that fit the observed proportion of $^{15}N^{+}$ cells at the end of the label-free chase are given in Table S1. In addition the estimated mean adipocyte lifetime was 70.3 (60.3, 78.9) weeks in the sWAT and 30.1 (26.7, 34.2) weeks in the vWAT. The parameters for the final model were as follows:

i) birth and death rate equal and constant over time

ii) preadipocyte label proportion underestimate of 56% in the sWAT and 0% in the vWAT

iii) fraction of adipocyte birth by differentiation without progenitor cell division of 100% in the sWAT and 46% in the vWAT

Supplemental References

Lechene, C., Hillion, F., McMahon, G., Benson, D., Kleinfeld, A.M., Kampf, J.P., Distel, D., Luyten, Y., Bonventre, J., Hentschel, D.*, et al.* (2006). High-resolution quantitative imaging of mammalian and bacterial cells using stable isotope mass spectrometry. J Biol *5*, 20.

Sjostrom, L., Bjorntorp, P., and Vrana, J. (1971). Microscopic fat cell size measurements on frozen-cut adipose tissue in comparison with automatic determinations of osmium-fixed fat cells. J Lipid Res *12*, 521-530.

Steinhauser, M.L., Bailey, A.P., Senyo, S.E., Guillermier, C., Perlstein, T.S., Gould, A.P., Lee, R.T., and Lechene, C.P. (2012). Multi-isotope imaging mass spectrometry quantifies stem cell division and metabolism. Nature *481*, 516-519.